

2006

Simple Method to Improve the Performance of Industrial Evaporators Under Frosting Conditions

Nawaf F. Aljuwayhel
University of Wisconsin

Douglas T. Reindl
University of Wisconsin

Sanford A. Klein
University of Wisconsin

Gregory F. Nellis
University of Wisconsin

Follow this and additional works at: <http://docs.lib.purdue.edu/iracc>

Aljuwayhel, Nawaf F.; Reindl, Douglas T.; Klein, Sanford A.; and Nellis, Gregory F., "Simple Method to Improve the Performance of Industrial Evaporators Under Frosting Conditions" (2006). *International Refrigeration and Air Conditioning Conference*. Paper 832. <http://docs.lib.purdue.edu/iracc/832>

This document has been made available through Purdue e-Pubs, a service of the Purdue University Libraries. Please contact epubs@purdue.edu for additional information.

Complete proceedings may be acquired in print and on CD-ROM directly from the Ray W. Herrick Laboratories at <https://engineering.purdue.edu/Herrick/Events/orderlit.html>

Simple Method to Improve the Performance of Industrial Evaporators Under Frosting Conditions

N. F. Aljuwayhel, D. T. Reindl*, S. A. Klein, and G. F. Nellis,
University of Wisconsin - Madison, 1500 Engineering Drive,
Madison, WI 53706, USA; Phone: 608/262-6381; dreindl@wisc.edu

ABSTRACT

This paper describes a theoretical model of a large-scale, ammonia-fed evaporator coil used in an industrial refrigeration system and operating under low temperature air and refrigerant conditions that are typically encountered in refrigerated storage spaces. The model is used to simulate the performance of counter- and parallel-flow circuited evaporator coil designs under frosting conditions. The counter-flow frost model is validated using in-situ data obtained from a field-installed evaporator coil. The performance of an evaporator in a parallel-flow circuit arrangement is simulated and compared to counter-flow circuiting. The effects of coil circuiting are evaluated in terms of the frost distribution across the evaporator coil and the associated reduction in cooling capacity.

1. INTRODUCTION

Frost will accumulate on the surfaces of evaporator coils that operate at temperatures below 0°C when the entering air dew point temperature is above the coil temperature. Frost accumulation is a serious problem that leads to a reduction in both the capacity and efficiency of a refrigeration system. The degradation in performance is related to the low conductivity of the frost layer which adds an additional thermal resistance between the air and the refrigerant and, more importantly, the reduction in air flow rate that is caused by the increased resistance to air flow through the narrowing channels due to the growing frost layer.

Counter-flow circuiting is largely used in all types of evaporator coils for industrial refrigeration, including direct expansion, natural recirculation and liquid overfed evaporators. One problem associated with using counter-flow circuiting for evaporator coils that operate under frosting conditions is that these evaporators will tend to accumulate more frost in the first few rows exposed to the incoming air. This concentration of the frost build up causes the flow resistance of the evaporator to increase rapidly which results in a corresponding, large reduction in the flow rate of air and refrigeration capacity. Such an evaporator will need to be defrosted quite often.

Many techniques have been proposed to reduce the frost accumulation rate thereby increasing the cooling operation time between defrost; for example, Ogawa et al. (1993) suggest modifications to the evaporator geometry such as the use of front fin staging, side fin staging and partially cut fins. Ogawa et al. showed that each of these techniques can be used to reduce the heat and mass transfer rates at the first few rows of evaporator coils. However, any of these techniques are penalized in that the refrigeration capacity provided by the modified evaporator coils during dry operation will be less than the dry capacity provided by the unmodified evaporator coils. Also, the modification to the geometry may be difficult to realize without adding substantial complexity to the fabrication process.

On the other hand, the current study shows that changing the circuiting of the evaporator tubes from counter-flow to parallel-flow (which can be done either by changing the refrigerant or the air flow direction) will result in an increase in the heat transfer rate of the dry coil as well as a more uniform distribution of the frost buildup and therefore a longer allowable cooling operation time between defrost.

2. FORMULATION OF THE MODEL

A liquid overfed evaporator coil consisting of multiple rows of finned tube with multiple refrigerant circuits (Figure 1) is considered. The model is formulated for a single refrigerant circuit that is assumed to be representative of the remaining (n) circuits in the coil. An individual evaporator circuit is divided into a number of sections that is equal

to the total number of the coil rows in the flow direction. The thermal properties of the freezer air are the inlet conditions associated with the first section. The outlet air and refrigerant properties for each section become the inlet properties for the next section (Figure 2).

The evaporator coil air-side heat transfer surfaces are rectangular plate fins that are modeled as equivalent circular fins each attached to a tube according to Schmidt (1949). The evaporator has a cross-flow configuration in which the direction of the air flow is perpendicular to the direction of the refrigerant flow. Almost all industrial evaporator coils are designed so that the refrigerant enters from the back-side of the evaporator coil (i.e., the air exit side) in what is referred to as a counter-flow arrangement, as shown in Figure 2. However, the present model is formulated so that the refrigerant inlet can be reversed allowing the refrigerant to enter from the front side of the evaporator coil (i.e., the air inlet side) in order to simulate a parallel flow arrangement. This small change in circuiting has a significant impact in the performance of the evaporator under frosting conditions, as discussed in section 4.

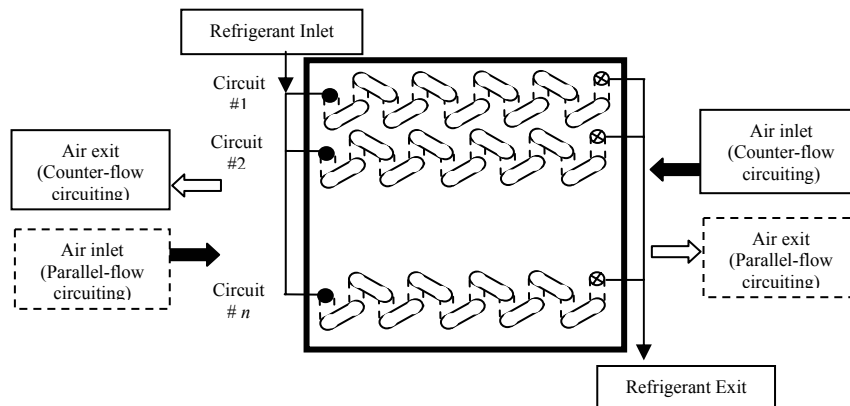


Figure 1 Schematic diagram showing evaporator coil with multiple rows of finned tubes with multiple refrigerant circuits and the direction of the air and the refrigerant flow for both the counter-flow and parallel-flow arrangements.

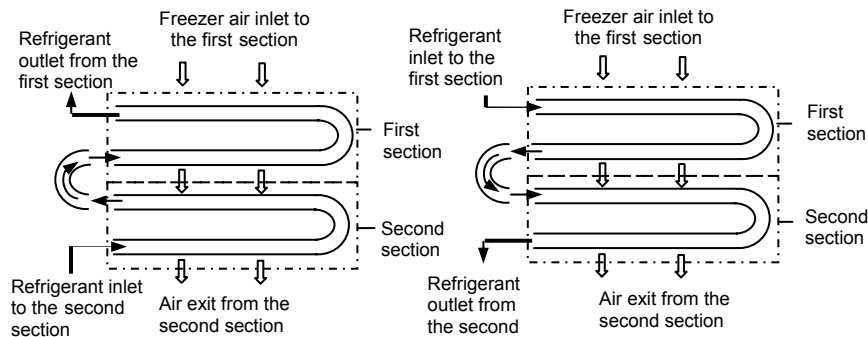


Figure 2 Schematic of the first and the second evaporator coil sections as well as the direction of the air and refrigerant flow for counter- (left) and, parallel-(right) flow arrangement.

2.1 Heat and Mass Transfer Equations

An energy balance relates the enthalpy reduction of the moist air stream to the increase in the enthalpy of the two-phase refrigerant within each section of the evaporator:

$$\dot{q}_{tot} = \dot{m}_a (i_{a,in} - i_{a,out}) = \dot{m}_r (i_{r,out} - i_{r,in}) \quad (1)$$

where \dot{m}_a and \dot{m}_r are the air and refrigerant mass flow rates, respectively, and $i_{a,in}$, $i_{a,out}$ and $i_{r,in}$ and $i_{r,out}$ are the inlet and outlet air and refrigerant enthalpies, respectively. The total heat transfer rate (\dot{q}_{tot}) is the sum of the sensible heat transfer rate, (\dot{q}_{sen}), and the latent heat transfer rate, (\dot{q}_{lat}). The sensible heat transfer rate is:

$$\dot{q}_{sen} = h_a A_e (T_{a,ave} - T_{f,ave}) \quad (2)$$

where (A_e) is the effective heat transfer area associated with the section, which is equal to the sum of the bare tubing surface area (A_b) and the fin surface area (A_{fin}) reduced by the total fin efficiency (η_{fc}):

$$A_e = A_b + \eta_{fc} A_{fin} \quad (3)$$

$T_{f,ave}$ and $T_{a,ave}$ are the average frost surface temperature and the average air dry bulb temperature within the section, respectively. The average air temperature is defined as:

$$T_{a,ave} = T_{r,ave} + \Delta T_{lm} \quad (4)$$

where $T_{r,ave}$ is the average refrigerant temperature and ΔT_{lm} is the log-mean temperature difference.

Because the typical air-cooling evaporator in an industrial refrigeration system is driven by a constant speed fan, the air mass (and volume) flow rate will decrease as frost accumulates and increases the flow resistance of the coil. As a consequence, the air-side convective heat transfer coefficient (h_a in Eq. (2)) will also change. In the model, the mass flow rate of air through the coil is fixed by the intersection of the evaporator's fan curve and the resistance curve associated with the frosted coil. Specific correlations for the air-side pressure drop or convective heat transfer coefficient associated with a frosted coil were not found. Rather, the pressure drop equation described in Kays et al. (1964) is used with a friction factor correlation suggested by McQuiston (1981). A correlation suggested by McQuiston (1981) is used to calculate the air-side convective heat transfer coefficient. These correlations were developed for a bare coil; however, the effect of the frost built up is approximately included by using the air mass flux based on the minimum free flow area and the local velocity considering the effect of the frost thickness.

The latent heat transfer rate is calculated using the mass transfer coefficient (h_m) defined by Threlkeld (1970).

$$h_m = \frac{h_a}{Le cp_a} \quad (5)$$

where (Le) is the Lewis number and (cp_a) is the specific heat of dry air. Lewis number is assumed to be 1.0. The latent heat transfer rate is calculated according to:

$$\dot{q}_{lat} = h_m i_{sg} A_e (\omega_{a,ave} - \omega_f) \quad (6)$$

where (i_{sg}) is heat of sublimation of water, and ($\omega_{a,ave}$) and (ω_f) are the average humidity ratio of the air and the saturation humidity ratio at the frost surface temperature, respectively. The average specific humidity of the air is calculated as suggested by Oskarsson et al. (1990):

$$\frac{\omega_{a,ave} - \omega_{a,in}}{\omega_{a,out} - \omega_{a,in}} = \frac{T_{a,ave} - T_{a,in}}{T_{a,out} - T_{a,in}} \quad (7)$$

Rearranging Eq. (6) so that it has the same form as Eq. (2) yields:

$$\dot{q}_{lat} = h_{lat} A_e (T_a - T_f) \quad (8)$$

where h_{lat} is the latent heat transfer coefficient which, can be expressed as:

$$h_{lat} = h_m i_{sg} \left(\frac{\omega_{a,ave} - \omega_f}{T_{a,ave} - T_f} \right) \quad (9)$$

The total heat transfer rate within any section of the heat exchanger is then:

$$\dot{q}_{tot} = \dot{q}_{sen} + \dot{q}_{lat} = (h_a + h_{lat}) A_e (T_{a,ave} - T_f) \quad (10)$$

The fin efficiency (η_f) for a circular fin with an adiabatic tip (Incropera and DeWitt (1990)) is:

$$\eta_f = \frac{2r_1}{m(r_2^2 - r_1^2)} \left[\frac{K_1(mr_1)I_1(mr_2) - K_1(mr_2)I_1(mr_1)}{I_0(mr_1)K_1(mr_2) + K_0(mr_1)I_1(mr_2)} \right] \quad (11)$$

where K_n and I_n are modified Bessel functions of the n^{th} order (the first and second kinds), r_1 and r_2 are the inner and outer radii of the equivalent circular fin, respectively, and m is the fin constant given by:

$$m = \sqrt{\frac{2 h_{eff}}{k_{fin} F_{thk}}} \quad (12)$$

where k_{fin} is the conductivity of the fin material, F_{thk} is the fin thickness and h_{eff} is the effective heat transfer coefficient. The effective heat transfer coefficient is defined so that it accounts for both latent and sensible heat transfer as well as for the conductive resistance of the frost layer:

$$h_{eff} = \left(\frac{1}{(h_a + h_{lat})} + \frac{\delta_f}{k_f} \right)^{-1} \quad (13)$$

where δ_f is the thickness of the frost layer and k_f is the average frost thermal conductivity which is calculated using the correlation developed by Lee et al. (1994). The inclusion of the latent heat transfer coefficient and the insulation effect of the frost in the fin efficiency, as described by Eqs. (12) and (13), was previously described by Kondepudi et al. (1993). A thermal contact resistance between the coil tubes and the fins (R_c) is included in the total fin efficiency (η_{fc}) using Eq. (14):

$$\eta_{fc} = \eta_f \left[1 + \eta_f A_{fin} h_{eff} \left(\frac{R_c}{A_{fin,c}} \right) \right]^{-1} \quad (14)$$

where $A_{fin,c}$ is the contact surface area between the coil tubes and fins. The value of the thermal contact resistance assumed is:

$$R_c = 0.0625 \times 10^{-4} (m^2 K/W) \quad (15)$$

The rate at which water vapor is transferred from the air stream to the coil surface (\dot{m}_f) is:

$$\dot{m}_f = \dot{m}_a (\omega_{a,in} - \omega_{a,out}) = h_m A_e (\omega_{a,ave} - \omega_f) \quad (16)$$

The frost layer density (ρ_f) at any time is calculated using a system of equations developed by Malhammar et al. (1988). The increase in the frost layer thickness ($\Delta\delta_f$) over a specific time interval of duration (Δt) is:

$$\Delta\delta_f = \frac{\dot{m}_f \Delta t}{A_{tot} \rho_f} \quad (17)$$

where (A_{tot}) is the total heat transfer area. Note that Eq. (17) implies that the frost will form uniformly over the tube and fin surface at any location; however, the model allows for the non-uniform buildup of frost through successive rows in the coil. The total heat transfer rate can finally be expressed as:

$$\dot{q}_{tot} = \frac{(T_{a,ave} - T_{r,ave})}{\frac{1}{(h_a + h_{lat}) A_e} + \frac{\delta_f}{k_f A_e} + \frac{R_{fa}}{A_e} + \frac{\ln(D_o/D_i)}{2\pi L k_{tube}} + \frac{1}{h_p A_i} + \frac{R_{fr}}{A_i}} \quad (18)$$

where k_{tube} is the thermal conductivity of the tubes and h_p is the refrigerant-side two-phase heat transfer coefficient, computed using a system of equations developed by Jung et al. (1989), and R_{fa} and R_{fr} are the fouling factor on the air and the refrigerant side, respectively. The fouling factors as suggested by Rosenhow et al. (1985) are:

$$R_{fa} = R_{fr} = 3.5 \times 10^{-4} (m^2 k/W) \quad (19)$$

Pressure drop on the refrigerant-side has typically been ignored in frost models (for example, Kondepudi et al. (1993) and Seker et al. (2004); however, the refrigerant-side pressure-drop plays a significant role in industrial evaporator coils because it produces a non-negligible temperature change on the refrigerant-side of the circuit which significantly affects the distribution of the frost formation and therefore the behavior of the coil under frosting conditions. The frictional pressure drop on the refrigerant-side within the straight tube sections is calculated using correlations developed by Muller, et al. (1986) and the inertial pressure drop associated with the flow of the two-phase refrigerant through the tube bends is calculated using correlations developed by Paliwoda (1992).

3. COUNTER-FLOW FROST MODEL VALIDATION

The equations and correlations described in the previous section are combined to form the evaporator model for both counter-flow and parallel-flow circuiting. The evaporator model developed is solved using Engineering Equation Solver (Klein (2006)). The predictions of the counter-flow frost model are compared and validated with experimental data obtained from a field experiment on an industrial air-cooling evaporator, the model showed good agreement with the measured cooling capacity, air flow rate, temperature difference between the inlet and the exit air streams and the total mass of accumulated frost; a discussion of the experiment and the resulting data are presented in Aljuwayhel et al. (2006). The details of the experimental evaporator coil are summarized in Table 1.

Table 1 Geometry and operating conditions of the coil used in the experiment

Parameter	Value	Parameter	Value
Fin pitch	0.85 cm (3/inch)	Fin/tube material	aluminum/carbon steel
Face area	8.23 m ² (88.56 ft ²)	Evaporation temperature	-34.4°C (-30°F)
Tube diameter	0.019 m (0.75 in)	Refrigerant	ammonia
Tube length	5.5 m (216 in)	Coil mass	3,900 kg (8,600 lbm)
Number of tubes	260	Nominal capacity	130 kW _T (37 tons)
Number of tube row	10	Number of fans	5
Tube transverse pitch,	0.057 m (2.25 in)	Horse power per fan	3.125 hp @-30F
Tube longitudinal pitch,	0.044 m (1.75 in)	Rated CFM	1,699 m ³ /min (60,000 cfm)

4. COUNTER-FLOW VERSUS PARALLEL-FLOW OPERATION

Figure 3 compares the evaporator cooling capacity predicted by the frost model using counter-flow and parallel-flow circuiting for otherwise the same evaporator geometry and operating conditions (Table 1). Figure 3 shows that there are several advantages associated with using the parallel-flow configuration as compared to the more conventional, counter-flow circuiting arrangement. The dry coil cooling capacity predicted for the parallel-flow circuiting (i.e., the capacity at the beginning of the simulation) is 8% higher than for the counter-flow arrangement; this observation agrees with the predictions of Nelson (1990), who suggested that there is a 3-4% performance advantage associated with a parallel-flow circuiting arrangement for liquid ammonia overfed evaporator coils operating under dry conditions.

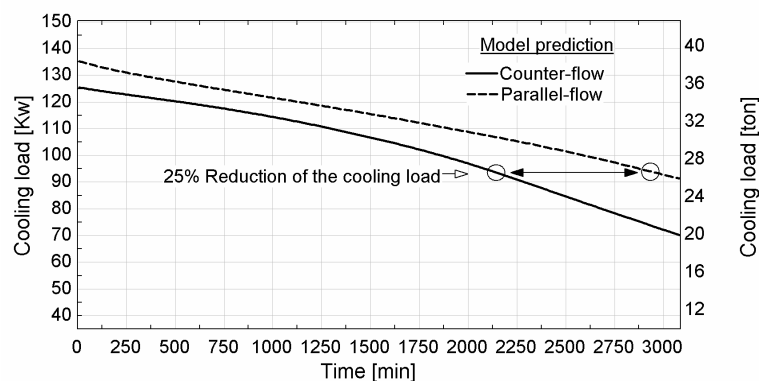


Figure 3 Comparison between the evaporator cooling capacity predicted by the counter-flow frost model and the parallel-flow frost model versus time.

The reason for the dry coil advantage is evident by observing the trends shown in Figure 4 and 5. Figure 4 shows a row-by-row comparison of the refrigerant temperature, air temperature, and the overall heat transfer coefficient at the beginning of the simulation (time = 0) for the (a) parallel- and (b) counter-flow arrangements. Figure 4(a) shows that the temperature difference between the ammonia and the air in a parallel-flow configuration decreases slightly for the coils that are deeper into the evaporator (i.e., coils with higher row numbers) whereas the overall heat transfer coefficient increases with row number. These effects balance and result in a nearly uniform distribution of the cooling load; as shown in Figure 5. The decrease in the refrigerant temperature is due to the decrease in refrigerant pressure associated with frictional and inertial pressure loss while the change in the overall heat transfer coefficient is due to the increase in the refrigerant quality as it evaporates. Figure 4(b) shows that the temperature difference between the ammonia and the air in a counter-flow configuration will decrease significantly with increasing coil rows as will the overall heat transfer coefficient. As a result, more of the cooling capacity will be provided by the first few coil rows, as shown in Figure 5.

Overall, the effectiveness of the counter-flow configuration is somewhat lower than the effectiveness of the parallel-flow configuration, which results in a slight reduction in the initial cooling capacity of the coil. It is interesting that this trend towards higher effectiveness for a parallel-flow configuration is exactly opposite of what is expected for a conventional heat exchanger; this counter-intuitive result occurs because the temperature of the refrigerant (which is increasing in enthalpy) will actually decrease in the direction of flow because of refrigerant-side pressure drop.

Another and potentially more significant advantage of the parallel-flow over the counter-flow circuiting arrangement arises due to the manner in which frost accumulates on the coil surface. The effectiveness advantage of the parallel-flow configuration tends to increase with time as frost accumulates; this effect is shown in Figure 3 where the predicted cooling capacity for the parallel-flow arrangement at the end of the simulation is 15% higher than the counter-flow arrangement. The improvement in the cooling performance under frosting conditions is primarily due to the characteristics of the frost accumulation and the associated effect on the air-side pressure drop. Just as the first few rows of the counter-flow configuration tend to supply most of the refrigeration, these rows also tend to accumulate most of the frost. Therefore, after the same amount of operating time, the minimum air-side flow area (which tends to dominate the flow resistance of the coil) for the counter-flow configuration will be much less than for the parallel-flow configuration and the air-side flow resistance will be much higher. Figure 6(a) shows the calculated air velocity as a function of time and illustrates that the air flow reduction due to frost buildup is substantially higher for the counter-flow configuration even though the total mass of the accumulated frost is actually slightly smaller (see Figure 6(b)).

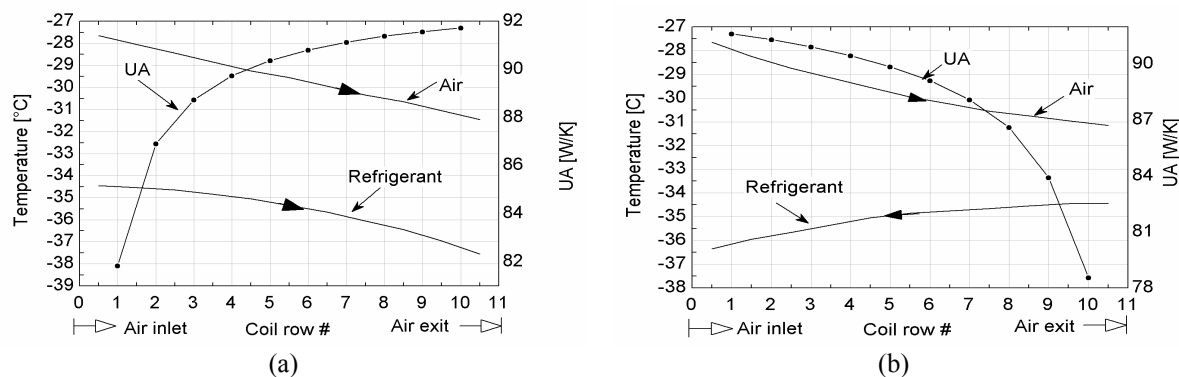


Figure 4 Predicted air and refrigerant temperature and UA across the evaporator coil for the (a) parallel-flow and (b) counter-flow configurations.

Figure 7 shows the percent blockage as a function of time for selected rows in the coil for the (a) counter- and (b) parallel-flow configurations; the counter-flow arrangement results in almost a 45% difference in the % blockage between the first and the last rows at the end of the simulation while there is only a 8.5% difference for the parallel-flow arrangement. Figure 7 shows that the first row of the counter-flow coil will reach 74% blockage at the end of the simulation as compared to only 58% blockage for the last row of the parallel-flow arrangement. This result clearly shows that parallel-flow evaporator coils can operate for a longer time before they must be defrosted. If, for example, the defrost cycle is initiated when the evaporator cooling capacity drops by 25%, then with the parallel-flow arrangements, the cooling mode period can be extended in time by 38% (13.5 hours), as shown in Figure 3.

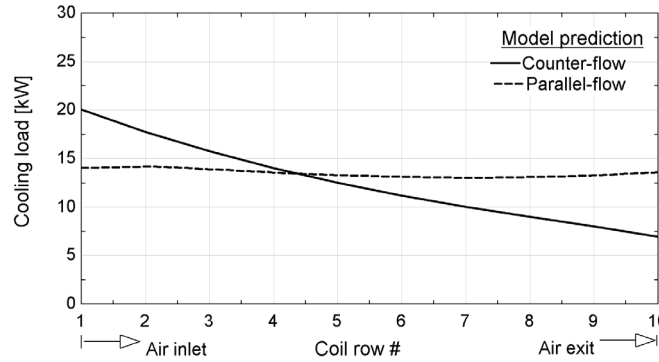


Figure 5 Cooling capacity across the evaporator for the counter-flow and parallel-flow configurations.

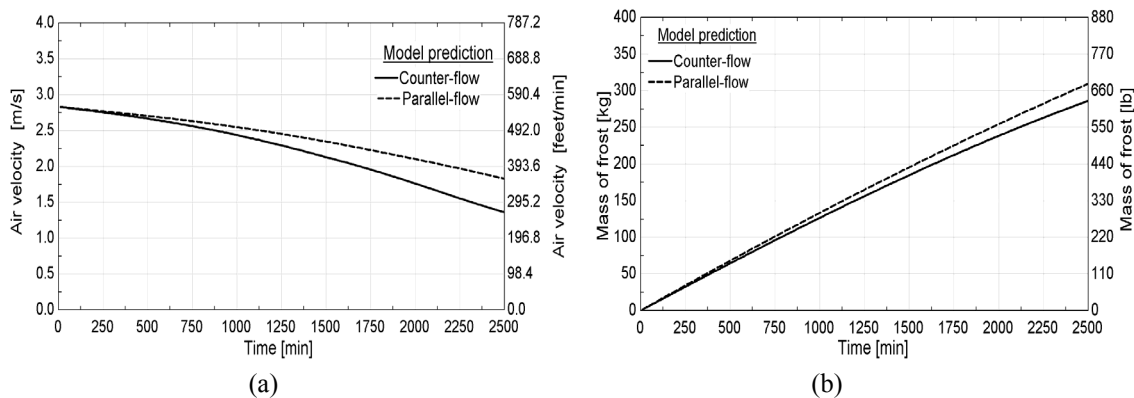


Figure 6 Comparison between the air velocity (a) and the total mass of the accumulated frost (b) predicted by the counter-flow and parallel-flow frost models over time.

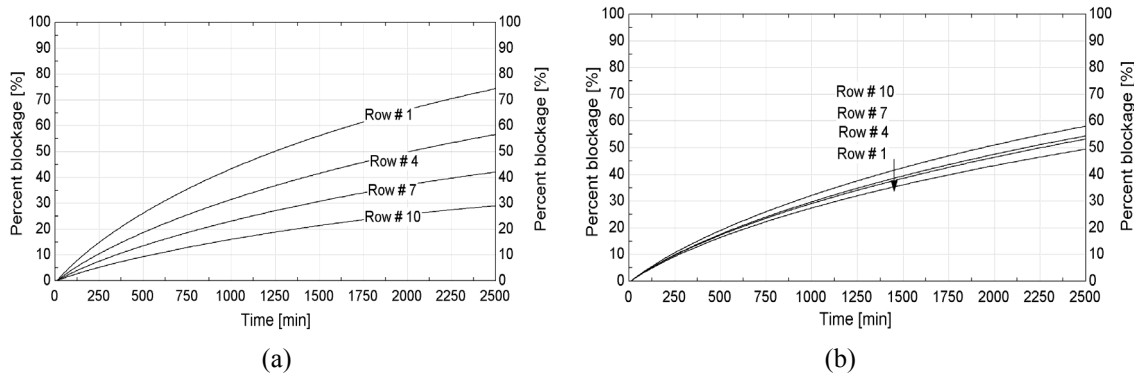


Figure 7 Percentage of the blockage of the air path caused by frost accumulation at different rows of the evaporator coil over time for (a) counter-flow and (b) parallel-flow circuiting.

5. CONCLUSION

This study shows there are two key advantages of the parallel-flow versus the counter-flow evaporator coils:

- The effectiveness of the counter-flow overfed industrial evaporator coils is slightly less than the effectiveness of the parallel-flow overfed industrial air-cooling evaporator coils and therefore the parallel-flow configuration provides slightly higher dry-coil cooling capacity.
- The cooling coil capacity advantage of the parallel-flow versus the counter-flow configuration tends to increase with time as frost accumulates. This is due primarily to the distribution of the accumulated frost

and its effect on the air-side pressure drop. Parallel-flow evaporator coils can be used for a significantly longer period of time before they must be defrosted.

NOMENCLATURE

A_b	Bare tube outside surface area (m ²)	i	Enthalpy (kJ kg ⁻¹)
A_{tot}	Total heat transfer area (m ²)	k_{fin}	Fin thermal conductivity (W m ⁻¹ K ⁻¹)
A_e	Effective heat transfer area (m ²)	k_f	Frost thermal conductivity (W m ⁻¹ K ⁻¹)
A_{fin}	Fin surface area (m ²)	k_{tube}	Tube thermal conductivity (W m ⁻¹ K ⁻¹)
A_i	Tube cross section area (m ²)	Le	Lewis number
cp_a	Specific heat for air (J kg ⁻¹ K ⁻¹)	\dot{m}	mass flow rate (kg s ⁻¹)
D_i	Tube inside diameter (m)	P_{fin}	Fin pitch (m)
D_o	Tube outside diameter (m)	P_t	Transverse tube pitch (m)
F_{thk}	Fin thickness (m)	P_r	Longitudinal tube pitch (m)
h_a	Convective air side heat transfer coefficient (W m ⁻² K ⁻¹)	r_1	Tube outside radius (m)
h_m	Mass transfer coefficient (kg m ⁻² s ⁻¹)	r_2	Fin equivalent radius (m)
h_{lat}	Latent heat transfer coefficient (W m ⁻² K ⁻¹)	T	Temperature (K)
h_{eff}	Effective air heat transfer coefficient (W m ⁻² K ⁻¹)		
h_{ip}	Refrigerant heat transfer coefficient (W m ⁻² K ⁻¹)		
	Greek symbols		Subscripts
ρ	Density (kg m ⁻³)	f	Frost
η_f	Fin efficiency	a	Air
η_{fc}	Fin efficiency including contact resistance	r	Refrigerant
ω	Specific humidity		
δ_f	Thickness of frost layer		

REFERENCES

- Aljuwayhel, N., Reindl, D., Klein, S., and Nellis, G., "Experimental Investigation of the Performance of Industrial Evaporator Coils Operating Under Frosting Conditions", submitted to *Int. J. Refrig.*, Jan, (2006).
- Incropera, F. and DeWitt, D. *Introduction to Heat Transfer*, John Wiley & Sons, 2nd edition, (1990).
- Jung, D. and Didion, D., "Horizontal Flow Boiling Heat Transfer Using Refrigerant Mixtures", *Electric Power Research Institute ER-6364*, EPRI Project 8006-2, (1989).
- Kays, W. and London, A., *Compact Heat Exchangers*, McGraw-Hill Book Company, New York, 1964.
- Klein, S. and Alvarado, F., *Engineering equation solver*, F-Chart Software, Middleton, WI, (2006).
- Kondepudi, S. and O'Neal, D., "Performance of Finned-Tube Heat Exchangers Under Frosting Conditions: Part I-Simulation Model", *Int. J. Refrig.*, Vol. 16, No. 3, (1993).
- Lee, K., Lee, T. and Kim, W., "Heat and Mass Transfer of Parallel Heat Exchanger under Frosting Conditions", *SAREK Journal*, Vol. 6, No. 2. (1994).
- Malhammar, A., "Monitoring Frost Growth in Evaporators is a Complex Process", *Australian Refrigeration, Air conditioning and Heat*, April, (1988).
- McQuiston, F., "Finned Tube Heat Exchangers: State of the Art for the Air-Side", *ASHRAE Transactions*, Vol. 87, No. 1, (1981).
- Nelson, B., "Design of Evaporators for Liquid Overfeed Systems", *ASHRAE Transactions*, Vol. 96, No. 1, (1990).
- Ogawa K., Tanaka N.O, Takeshita M., "Performance improvement of plate fin-and-tube heat exchangers under frosting conditions", *ASHRAE Transaction*, Vol. 99, No. 1, (1993).
- Oskarsson, S. and Krakow, K., "Evaporator Models for Operation with Dry, Wet and Frosted Finned Surfaces - Part I&II", *ASHRAE Transactions*, Vol. 96, No. 1, (1990).
- Rosenhow, W.M., Hartnett, J.P., and Ganic, E.N., *Handbook of heat transfer applications*, 2nd ed. New York: McGraw Hill. (1985).
- Seker, D., Karatas, H., and Egrican, N., "Frost Formation on Fin-and-Tube Heat Exchangers: Part I&II", *Int. J. Refrig.*, Vol. 27, No. 4, (2004).
- Schmidt, T., "Heat Transfer Calculation for Extended Surfaces", *Refrigerating Engineering*, Vol. 57, (1949).
- Threlkeld, J., *Thermal Environmental Engineering*, Prentice Hall Book Co., Englewood Cliffs, NJ, 2nd edition, (1970).